EFFICIENT INVERSION OF THE CONE BEAM TRANSFORM FOR A GENERAL CLASS OF CURVES

A. KATSEVICH AND M. KAPRALOV

Abstract. We extend an efficient cone beam transform inversion formula, proposed earlier by one of the authors for helices, to a general class of curves. The conditions that describe the class are very natural. Curves C are smooth, without self-intersections, have positive curvature and torsion, do not bend too much, and do not admit lines which are tangent to C at one point and intersect C at another point. The notions of PI-lines and PI-segments are generalized, their properties are studied. The domain U is found, where PI-lines are guaranteed to be unique. Results of numerical experiments demonstrate very good image quality.

1. Introduction

Image reconstruction from projections is important both in pure mathematics (as a problem of integral geometry) and in applications (as a problem of computed tomography (CT)). Cone beam CT is one of the most common medical imaging modalities. Here one recovers a function $f(x), x \in \mathbb{R}^3$, knowing the integrals of f along lines that intersect a curve C. The curve C is usually called a source trajectory. The ever-increasing needs of medical imaging require the development of inversion algorithms for more and more general source trajectories.

A number of theoretically exact algorithms have been proposed in the past several years. They can be classified into three groups: filtered backprojection (FBP) algorithms, slow-FBP algorithms, and backprojection filtration (BPF) algorithms. Slow-FBP and BPF algorithms are quite flexible, allow some transverse data truncation, and can be used for virtually any complete source trajectory [PN05, PNC05, ZPXW05, SZP05, YZYW05b, YZYW05a, ZLNC04]. FBP algorithms are less flexible, but they are by far the fastest and have been developed for a range of source trajectories. They include constant pitch helix [Kat02, Kat04b, Kat04c, Kat06], dynamic pitch helix [KBH04, KK06], circle-and-line [Kat04a], circle-and-arc [Kat05, CZLN06], and saddle [YLKK06]. Significant progress has also been achieved in the development of quasi-exact algorithms [BKP05, KBK06].

As the list presented above shows, until now FBP algorithms have been proposed only for certain types of well-defined trajectories: helices, saddles, etc. There was no FBP algorithm for a general class of curves. Ideally, such a class would be described only in terms of some basic geometric properties (e.g., smoothness, curvature, etc.) rather than specifying the types of curves (helices, etc.). In this paper we develop a theoretically exact shift-invariant FBP algorithm for a wide class of source trajectories. The conditions describing our class are very natural.

The work of the two authors was supported in part by NSF grant DMS-0505494
Department of Mathematics, University of Central Florida, Orlando, FL 32816-1364
E-mail address: mikhail@mail.ucf.edu, akatsevi@pegasus.cc.ucf.edu.

We consider curves C that are smooth, have no self-intersections, have positive curvature and torsion, do not bend too much, and do not admit lines which are tangent to C at one point and intersect C at another point. Our algorithm applies to any curve with these properties. The inversion algorithm of this paper is a generalization of the formula proposed for constant- and variable-pitch helices in [Kat02, Kat04b, KBH04].

The importance of our results is two-fold. First, the algorithm can be used in a variety of applications. For example, in electron-beam CT/micro-CT there arise source trajectories that can be described as helices with variable radius and pitch [YZW04]. No efficient FBP algorithm existed for such curves, but the new one does apply. Nice first steps towards adapting the inversion formula of [Kat02, Kat04b, KBH04] to these curves were obtained in [YZW04]. Second, the results have theoretical value as well. They provide a deeper understanding of the available algorithms, put them into the context of a more general approach, and demonstrate which geometrical properties the curve is required to have for the FBP algorithm to apply.

The paper is organized as follows. In Section 2 we define PI-lines for general curves, describe precisely the class of curves considered in the paper, and study properties of their PI-segments. In Section 3 we find the set U where PI-lines are guaranteed to be unique. The result is based on the notions of maximal and minimal PI-lines. These critical PI-lines can be viewed as a generalization of the axial direction for regular helices. Also we find the special planes, such that the stereographic projection of C onto these planes has very useful properties. In Section 4 we study more properties of the PI-segments of C. Then the inversion formula is given. Finally, the results of numerical experiments are presented in Section 5.

2. PI lines and their properties

The objective of this section is to define PI lines for a general class of smooth curves and study their properties. Let C be a smooth curve:

$$I := [a,b] \ni s \to y(s) \in \mathbb{R}^3,\ |\dot{y}(s)| \neq 0. \tag{2.1}$$

Here and below the dot above a variable denotes differentiation with respect to s. Define the functions

$$\Phi(s,s_0) := [y(s)-y(s_0), \dot{y}(s), \ddot{y}(s)],\ Q(s,s_0) := [y(s)-y(s_0), \dot{y}(s_0), \dot{y}(s)], \tag{2.2}$$

where $[e_1,e_2,e_3] := e_1 \cdot (e_2 \times e_3)$ denotes the scalar triple product of three vectors. If C is a helix, then Φ and Q are precisely the functions that have been introduced under the same names in [KBH04]. Similarly to [KBH04], it turns out later that Φ is intimately related to the convexity of the projection of C onto a detector plane (cf. (4.7) below), and Q is related to the uniqueness of PI-lines (cf. Definitions 2.1, 2.2, equation (3.6), and the proof of Proposition 3.2). Given any $s_0, s_1 \in I$, $H(s_0,s_1)$ denotes the line segment with the endpoints $y(s_0), y(s_1) \in C$.

Definition 2.1. *Pick two points $y(s_0), y(s_1) \in C$, $s_0 < s_1$. The line segment $H(s_0,s_1)$ is called the PI-segment if $Q(s,q) \neq 0$ for any $s,q \in [s_0,s_1]$, $s \neq q$.*

Definition 2.2. *Pick two points $y(s_0), y(s_1) \in C$, $s_0 < s_1$. The line segment $H(s_0,s_1)$ is called the maximal PI-segment if $Q(s_0,s_1) = 0$, but $Q(s,q) \neq 0$ for any $s,q \in (s_0,s_1)$, $s \neq q$.*

If C is a helix, definition 2.1 gives the usual PI-segments $H(s,q), 0 < q-s < 2\pi$, and definition 2.2 gives the maximal PI-segments $H(s, s+2\pi)$.

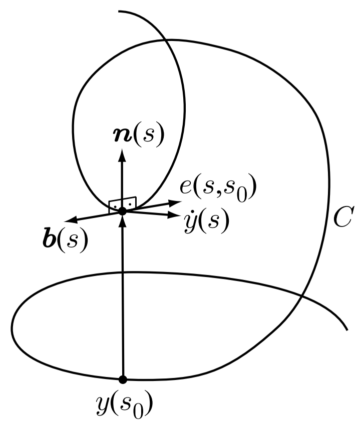

FIGURE 1. Critical case

Next we discuss how a smooth curve bends. Consider two points: $y(s_0), y(s) \in C$. Assume $y(s_0)$ is fixed, and $y(s)$ moves along C. The line segment joining $y(s_0)$ and $y(s)$ rotates about the instantaneous axis $e(s,s_0) = (y(s)-y(s_0)) \times \dot{y}(s)/|(y(s)-y(s_0)) \times \dot{y}(s)|$. The point $y(s)$ rotates also about the instantaneous axis, which is obtained by finding the circle of curvature of C at $y(s)$ (also known as the osculating circle). The corresponding axis of rotation is $\mathbf{b}(s)$, i.e. the binormal vector. If $s \to s_0$, then $e(s,s_0) \to \mathbf{b}(s)$. Thus, the difference in directions of the two vectors can measure how much the curve bends between the two points. The maximum possible "bent" occurs when the two axes point in the opposite directions: $e(s,s_0) = -\mathbf{b}(s)$ (see Figure 1).

Now we can formulate the main assumptions on the curve C.

- C1. C is smooth, and the curvature and torsion of C are positive;
- C2. C does not self-intersect within any PI-segment (or a maximal PI-segment) of C;
- C3. Given any PI-segment (or a maximal PI-segment) $H(s_0,s)$ of C, there is no line tangent to C at $y(s_1)$ and intersecting C at $y(s_2)$ with $s_1, s_2 \in [s_0, s]$, $s_1 \neq s_2$;
- C4. C does not bend too much, i.e. given any PI-segment (or a maximal PI-segment) $H(s_0,s)$ of C, one has $e(s_1,s_2) \neq -\mathbf{b}(s_2)$ for any $s_1, s_2 \in [s_0, s]$, $s_1 \neq s_2$.

If a curve satisfies conditions C1–C4, then its PI-segments have a number of nice properties.

Proposition 2.3. *Let C be a curve, which satisfies conditions C1–C4, and let $H(s_0,s_1)$ be its (possibly maximal) PI-segment. Then for any $s,q \in [s_0,s_1]$ one has: $\Phi(s,q) > 0$ if $s > q$ and $\Phi(s,q) < 0$ if $s < q$.*

Proof. By shrinking the PI-line if necessary, the proposition follows if we show that $\Phi(s,s_0) \neq 0$ for any $s \in (s_0,s_1]$ and $\Phi(s,s_1) \neq 0$ for any $s \in [s_0,s_1)$. We prove only the first statement, because the proof of the second one is analogous.

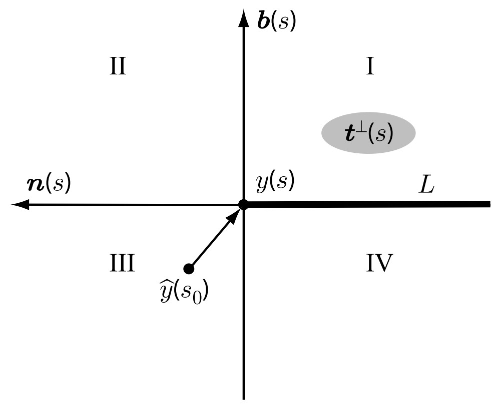

FIGURE 2. Projection of $y(s_0)$ onto the plane through $y(s)$ with normal vector $\dot{y}(s)$

Let us assume that the parameterization of $y(s)$ is natural, i.e. $|\dot{y}(s)| \equiv 1$. For convenience, recall the Frenet-Serret formulas:

$$\begin{bmatrix} \dot{\mathbf{t}} \\ \dot{\mathbf{n}} \\ \dot{\mathbf{b}} \end{bmatrix} = \begin{bmatrix} 0 & \kappa & 0 \\ -\kappa & 0 & \tau \\ 0 & -\tau & 0 \end{bmatrix} \begin{bmatrix} \mathbf{t} \\ \mathbf{n} \\ \mathbf{b} \end{bmatrix}, \tag{2.3}$$

where $\mathbf{t}(s), \mathbf{n}(s), \mathbf{b}(s)$ are the unit tangent, normal and binormal vectors, respectively, $\kappa(s)$ is the curvature and $\tau(s)$ is the torsion of the source trajectory. Using (2.3), we get

$$\begin{aligned} \Phi(s, s_0) = [y(s) - y(s_0), \dot{y}(s), \ddot{y}(s)] &= \kappa(s)[y(s) - y(s_0), \mathbf{t}(s), \mathbf{n}(s)] \\ &= \kappa(s)\mathbf{b}(s) \cdot (y(s) - y(s_0)). \end{aligned} \tag{2.4}$$

Since we are interested in the sign of $\Phi(s, s_0)$ and $\kappa(s) > 0$, we determine the sign of

$$\begin{aligned} \mathbf{b}(s) \cdot (y(s) - y(s_0)) &= \int_{s_0}^{s} (\mathbf{b}(t) \cdot (y(t) - y(s_0)))'_t \, dt \\ &= -\int_{s_0}^{s} \tau(t)\mathbf{n}(t) \cdot (y(t) - y(s_0)) dt. \end{aligned} \tag{2.5}$$

Let $\mathbf{t}^{\perp}(s)$ denote the plane passing through $y(s)$ and perpendicular to $\mathbf{t}(s)$. We assume that $\mathbf{n}(s)$ and $\mathbf{b}(s)$ are the coordinate axes on the plane, and $y(s)$ is the origin (see Figure 2).

Let $\Pi_{osc}(s)$ denote the osculating plane of C at $y(s)$. Recall that $\Pi_{osc}(s)$ contains $y(s)$ and is parallel to $\dot{y}(s)$ and $\ddot{y}(s)$. If $y(s_0)$ projects onto the ray $L := y(s) - \lambda\mathbf{n}(s), \lambda > 0$, then $y(s_0)$ belongs to $\Pi_{osc}(s)$. Moreover, the two rotation axes: one, determined by rotation of $y(s)$ around $y(s_0)$, and the other, $\mathbf{b}(s)$ - determined by rotation of $y(s)$ relative to the intrinsic center of rotation, are parallel and point in the opposite directions. This is prohibited by the assumption that the curve does not bend too much, so $y(s_0)$ never projects onto L.

Let $\hat{y}(s_0)$ denote the projection of $y(s_0)$ onto $\mathbf{t}^{\perp}(s)$. The Taylor series expansions shows that $\tau > 0$ and $\kappa > 0$ imply

$$\mathbf{n}(t) \cdot (y(s) - y(s_0)) < 0, \;\; \mathbf{b}(s) \cdot (y(s) - y(s_0)) > 0, \tag{2.6}$$

for $s - s_0 > 0$ small enough. Hence, initially $\hat{y}(s_0)$ is located in the third quadrant (see Figure 2). Suppose now s increases. If $\hat{y}(s_0)$ appears in the third quadrant, then $\mathbf{n}(t) \cdot (y(t) - y(s_0)) < 0$. So $\mathbf{b}(s) \cdot (y(s) - y(s_0))$ increases, $\hat{y}(s_0)$ moves down and does not cross the $\mathbf{n}$-axis. If $\hat{y}(s_0)$ appears in the fourth quadrant, then $\mathbf{n}(t) \cdot (y(t) - y(s_0)) > 0$ and $\mathbf{b}(s) \cdot (y(s) - y(s_0))$ decreases. This implies that in the fourth quadrant $\hat{y}(s_0)$ moves up. However, our assumption precludes $\hat{y}(s_0)$ from crossing L. Consequently, $\hat{y}(s_0)$ never crosses the $\mathbf{n}$-axis and $\Phi(s, s_0) > 0$ for any $s \in (s_0, s_1]$. □

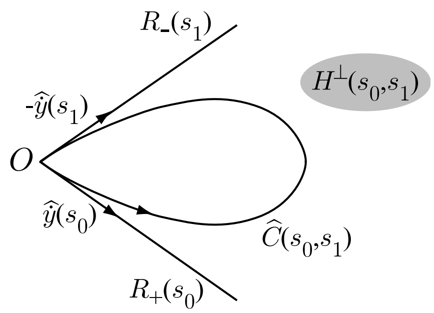

FIGURE 3. Illustration of the containment property: orthogonal projection onto $H^{\perp}(s_0, s_1)$

Let $H(s_0, s_1)$ be a PI-segment (possibly maximal), and $C(s_0, s_1)$ the corresponding curve segment. Project $C(s_0, s_1)$, $\dot{y}(s_0)$, and $\dot{y}(s_1)$ orthogonally onto a plane perpendicular to $H(s_0, s_1)$. Such a plane is denoted $H^{\perp}(s_0, s_1)$. The corresponding projections are denoted $\hat{C}(s_0, s_1)$, $\hat{\dot{y}}(s_0)$, and $\hat{\dot{y}}(s_1)$, respectively (see Figure 3). Let O be the projection of $H(s_0, s_1)$. The vectors $\hat{\dot{y}}(s_0)$ and $\hat{\dot{y}}(s_1)$ determine two rays:

$$\begin{aligned} R_{+}(s_0) &:= \{x \in H(s_0, s_1)^{\perp} : x = O + \lambda \hat{\dot{y}}(s_0), \lambda \geq 0\}, \\ R_{-}(s_0) &:= \{x \in H(s_0, s_1)^{\perp} : x = O + \lambda(-\hat{\dot{y}}(s_1)), \lambda \geq 0\}. \end{aligned} \tag{2.7}$$

Proposition 2.4. *Let C be a curve, which satisfies conditions C1–C4. If $H(s_0, s_1)$ is a (possibly maximal) PI-segment of C, then one has:*

1. *$\hat{C}(s_0, s_1)$ is contained inside the wedge with vertex O and formed by the rays $R_{+}(s_0)$ and $R_{-}(s_1)$;*
2. *$\hat{C}(s_0, s_1)$ is smooth and no line through O is tangent to $\hat{C}(s_0, s_1)$ at an interior point;*
3. *If $H(s_0, s_1)$ is not maximal, the angle between $R_{+}(s_0)$ and $R_{-}(s_1)$ is less than π. If $H(s_0, s_1)$ is maximal, the angle between the rays equals π;*
4. *No line through O intersects the interior of $\hat{C}(s_0, s_1)$ at more than one point.*

The property of C described in statement (1) of the proposition is important for us, so it will be given the name *containment property*. In other words, statement (1) says that PI-segments of curves, which satisfy conditions C1–C4, have the containment property.

Proof. To show that $\hat{C}(s_0, s_1)$ is contained inside the wedge, we first consider $\hat{C}(s_0, s)$, where $s = s_0 + \epsilon$ for some $0 < \epsilon \ll 1$. As is easily seen, containment follows from the two inequalities:

$$\begin{aligned} &[y(t)-y(s_0), y(s_1)-y(s_0), \dot y(s_0)] > 0\ \forall t\in(s_0,s_1),\\ &[y(t)-y(s_0), y(s_1)-y(s_0), \dot y(s_1)] > 0\ \forall t\in(s_0,s_1). \end{aligned} \tag{2.8}$$

To prove the first inequality introduce the function

$$\Psi(s_1,t) := \left[\frac{y(t)-y(s_0)-\dot y(s_0)(t-s_0)}{(t-s_0)^2}, \frac{y(s_1)-y(s_0)-\dot y(s_0)(s_1-s_0)}{(s_1-s_0)^2}, \dot y(s_0)\right]. \tag{2.9}$$

By using the Taylor series expansions we see that $\Psi(s_1,t)$ is smooth and bounded on compact sets. Notice also that

$$\Psi(s_1,s_1)=0,\ \ \Psi_t'(s_1,t)<\infty. \tag{2.10}$$

Hence $\Psi(s_1,t)/(s_1-t)$ is bounded as well, which implies

$$\begin{aligned} &[y(t)-y(s_0), y(s_1)-y(s_0), \dot y(s_0)]\\ &\quad = \frac{(t-s_0)^2(s_1-s_0)^2(s_1-t)}{12}([\dot y(s_0), \ddot y(s_0), \dddot y(s_0)] + o(1)) > 0, \end{aligned} \tag{2.11}$$

where $o(1)\to 0$ as $s_1\to s_0$. The second inequality in (2.8) can be proven for small $s_1-s_0>0$ in a similar fashion.

Suppose now s_1-s_0 is not necessarily small. Note that $\hat C(s_0,s_1)$ is tangent to the rays $R_+(s_0)$ and $R_-(s_1)$ at the point O of order precisely one. Consider, for example, the ray $R_+(s_0)$. To determine the order of tangency we need to find the asymptotics of the first expression in (2.8) as $t\to s_0$, with s_0 and s_1 fixed. We have:

$$\begin{aligned} &[y(t)-y(s_0), y(s_1)-y(s_0), \dot y(s_0)]\\ &\quad = [\ddot y(s_0), y(s_1)-y(s_0), \dot y(s_0)]\frac{(t-s_0)^2}{2} + O\left((t-s_0)^3\right)\\ &\quad = -\Phi(s_0,s_1)\frac{(t-s_0)^2}{2} + O\left((t-s_0)^3\right). \end{aligned} \tag{2.12}$$

Similarly,

$$[y(t)-y(s_0), y(s_1)-y(s_0), \dot y(s_1)] = \Phi(s_1,s_0)\frac{(t-s_1)^2}{2} + O\left((t-s_1)^3\right),\ t\to s_1. \tag{2.13}$$

By Proposition 2.3, $\Phi(s_0,s_1)<0$, $\Phi(s_1,s_0)>0$, and the desired assertion follows.

Suppose $C(s_0,s_1)$ does not have the containment property. Assume, for example, that the first inequality in (2.8) is violated. A violation of the other inequality can be considered analogously. From (2.12) and Proposition 2.3, the inequality holds for some $t>s_0$, where $t-s_0$ is sufficiently small. Thus there exists $t\in(s_0,s_1)$ such that

$$[y(t)-y(s_0), y(s_1)-y(s_0), \dot y(s_0)] = 0. \tag{2.14}$$

Equation (2.14) defines t as a function of s_1. Differentiating (2.14) with respect to s_1 gives:

$$\frac{dt}{ds_1} = -\frac{[y(t)-y(s_0), \dot y(s_1), \dot y(s_0)]}{[\dot y(t), y(s_1)-y(s_0), \dot y(s_0)]}. \tag{2.15}$$

The denominator in (2.15) does not vanish. Otherwise, from the linear independence of $\dot y(s_0)$ and $y(s_1)-y(s_0)$ (property C3) and (2.14) we get $Q(t,s_0) =$

$[y(t) - y(s_0), \dot{y}(s_0), \dot{y}(t)] = 0$. Since $H(s_0, s_1)$ is a PI-line, this is a contradiction. Hence we can consider the function $t(s)$ for some $s \le s_1$ using that $Q(t, s_0) \ne 0$ for $t \in (s_0, s_1)$. As s decreases from s_1 towards s_0, one of the following must happen:

a) $s, t \to s^* \ne s_0$. Replacing s_1 with s, and t - with $t(s)$ in (2.14) gives $Q(s^*, s_0) = [y(s^*) - y(s_0), \dot{y}(s_0), \dot{y}(s^*)] = 0$, which contradicts the assumption that $H(s_0, s_1)$ is a PI-line.

b) $t \to s_0$, $s \to s^* > s_0$. From (2.14), $\Phi(s_0, s^*) = [y(s_0) - y(s^*), \dot{y}(s_0), \ddot{y}(s_0)] = 0$, which contradicts Proposition 2.3.

Note that $s, t \not\to s_0$ because of (2.11). Thus the containment property is established.

To prove the second statement we argue by contradiction. Suppose there exists $t \in (s_0, s_1)$, where either $\hat{C}(s_0, s_1)$ is non-smooth or where the line through O and $\hat{y}(t)$ is tangent to $\hat{C}(s_0, s_1)$. Here $\hat{y}(t)$ is the projection of $y(t)$ onto $H^{\perp}(s_0, s_1)$. In both cases

$$[y(s_1) - y(s_0), \dot{y}(t), y(t) - y(s_0)] = 0. \tag{2.16}$$

Just as in the proof of statement (1), (2.16) defines t as a function of s_1. Differentiating (2.16) with respect to s_1 gives:

$$\frac{dt}{ds_1} = -\frac{[\dot{y}(s_1), \dot{y}(t), y(t) - y(s_0)]}{[y(s_1) - y(s_0), \ddot{y}(t), y(t) - y(s_0)]}. \tag{2.17}$$

The denominator in (2.17) does not vanish. Otherwise, together with (2.16) this gives $\Phi(t, s_0) = [y(t) - y(s_0), \dot{y}(t), \ddot{y}(t)] = 0$, which contradicts Proposition 2.3. Here we have used the fact that $y(s_1) - y(s_0)$ and $y(t) - y(s_0)$ are not parallel (cf. (2.8)). Hence we can consider the function $t(s)$ for some $s \le s_1$ using that $\Phi(t, s_0) \ne 0$ for $t \in (s_0, s_1]$. As s decreases from s_1 towards s_0, one of the following must happen:

a) $s, t \to s^* \ne s_0$. Replacing s_1 with s and t with $t(s)$ in (2.16) gives $[y(s^*) - y(s_0), \dot{y}(s^*), \ddot{y}(s^*)] = 0$, which contradicts Proposition 2.3.

b) $t \to s_0$, $s \to s^* > s_0$. Then (2.16) implies $[y(s^*) - y(s_0), \dot{y}(s_0), \ddot{y}(s_0)] = 0$, which is again a contradiction.

c) $s, t \to s_0$. Now (2.16) implies $[\dot{y}(s_0), \ddot{y}(s_0), \dddot{y}(s_0)] = 0$, i.e. $\tau(s_0) = 0$. This contradicts the assumption $\tau(s_0) > 0$.

Our argument proves that (2.16) does not happen, so statement (2) is established.

To prove statement (3), first consider $H(s_0, q)$ for $q - s_0 > 0$ sufficiently small. As follows from statements (1) and (2), $\hat{C}(s_0, q)$ is contained between the rays $R_+(s_0)$ and $R_-(q)$, which are close to each other. As q increases towards s_1, the two rays cannot collapse into one. Because of the containment, $\hat{C}(s_0, q)$ is always located between the rays. So if the two rays collapse into one for some $q > s_0$, then $C(s_0, q)$ is a planar curve, which contradicts the assumption $\tau > 0$. Hence $Q(s_0, s_1) = 0$ if and only if $R_+(s_0)$ and $R_-(s_1)$ point in the opposite directions (see Figure 5).

Statements (1)–(3) imply that (i) whenever a line through O intersects $\hat{C}(s_0, s_1)$, then all the intersection points (IPs) are on one side of O; and (ii) neither $R_+(s_0)$ nor $R_-(s_1)$ intersects the interior of $\hat{C}(s_0, s_1)$. By (i) we can replace "line" with "ray" in statement (4). Suppose there is a ray γ with vertex at O, which intersects $\hat{C}(s_0, s_1)$ at two interior points. Clearly, by rotating γ around O towards either $R_+(s_0)$ or $R_-(s_1)$ we can make the two IPs collide. As soon as the IPs collide, we get a ray tangent to $\hat{C}(s_0, s_1)$ at an interior point, which contradicts statement (2). $\square$

Corollary 2.5. *No plane intersects $C(s_0, s_1)$ at more than three points.*

Proof. Suppose there is a plane Π that has at least four IPs with $C(s_0, s_1)$: $s_0 \le t_1 < t_2 < t_3 < t_4 \le s_1$. Consider $C(t_1, t_4)$ and project it onto the plane perpendicular to $H(t_1, t_4)$ (as was done in the proof of Proposition 2.4). As before, let O denote the projection of $H(t_1, t_4)$. The projection of Π gives the line through O, which intersects $\hat{C}(t_1, t_4)$ at least at two points, which contradicts statement (3) of Proposition 2.4. □

Corollary 2.6. *Pick any $x \in H(s_0, s_1)$ and $s \in (s_0, s_1)$. Consider a plane Π rotating around the axis $\beta(s, x)$. The number of IPs of Π and $C(s_0, s_1)$ changes from one to three when Π passes through $H(s_0, s_1)$.*

Proof. Consider the critical case when Π contains $H(s_0, s_1)$. As follows from Proposition 2.4, the vectors $\dot{y}(s_0)$ and $-\dot{y}(s_1)$ point into the opposite half-planes relative to Π. Hence, a small rotation of Π around $\beta(s, x)$ in one direction gives 1IP, and in the opposite direction - 3IPs. See Section 4 in [Kat06] for more details. □

3. Establishing uniqueness of PI lines

To establish uniqueness of PI lines, we generalize the standard argument from helices [KND00, KL03, KBH04] to general curves.

Fix $x \in U$. For each $s \in I$, fix a vector $N(s)$, $|N(s)| \equiv 1$ (a specific $N(s)$ will be chosen later). Define the functions $q(s)$ and $\lambda(s)$ so that $q(s) > s$, $H(s, q(s))$ is a PI-segment, $0 < \lambda(s) < 1$, and the point

$$x(s) := y(s) + \lambda(s)(y(q(s)) - y(s)) \in H(s, q(s)) \tag{3.1}$$

has the property

$$x(s) - x \parallel N(s). \tag{3.2}$$

We assume that the functions $q(s)$ and $\lambda(s)$ with the required properties exist. Later (see (3.10) and the proof of Proposition 3.2) we find U such that for any $x \in U$ the functions $q(s)$ and $\lambda(s)$ do exist.

Condition (3.2) means that the parallel projection of $x(s)$ onto the plane through x with normal vector $N(s)$ coincides with x. Note that the vector-valued function $N(s)$ is determined independently of $q(s)$ and $\lambda(s)$. A similar idea is used in proving the uniqueness of PI lines for the standard helix, the difference being that the vector $N(s)$ is constant and directed along the axis of the helix.

Figure 4 illustrates the setup: the functions $q(s)$ and $\lambda(s)$ are defined in such a way as to ensure that the parallel projection of $x(s)$ onto the plane through x with normal $N(s)$ always coincides with x. Denote $\Delta y(s) := y(q(s)) - y(s)$. Thus,

$$\varepsilon(s) := N(s) \cdot \{(y(s) + \lambda(s)\Delta y(s)) - x\} \tag{3.3}$$

is the signed distance from $y(s) + \lambda(s)\Delta y(s)$ to x, i.e. $\varepsilon(s) = 0$ if and only if the chord $H(s, q(s))$ passes through x. We are interested in calculating $\varepsilon'(s)$.

Combining (3.1)–(3.3) gives

$$y(s) + \lambda(s)(y(q(s)) - y(s)) = x + \varepsilon(s)N(s). \tag{3.4}$$

Differentiate (3.4) with respect to s:

$$\dot{y}(s) + \lambda'(s)\Delta y(s) + \lambda(\dot{y}(q(s))q'(s) - \dot{y}(s)) = \varepsilon'(s)N(s) + \varepsilon(s)\dot{N}(s). \tag{3.5}$$

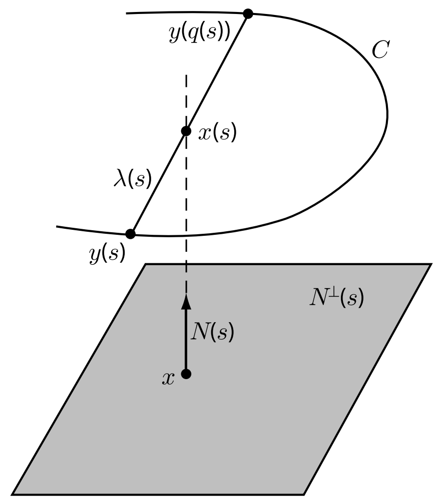

FIGURE 4. Parallel projection onto the plane $N^{\perp}(s)$ through x

Computing the dot product of (3.5) with $\Delta y(s) \times \dot{y}(q)$ on both sides gives the expression:

(3.6)
$$\varepsilon'(s) = A(s) + \varepsilon(s)B(s),$$
$$A(s) := -(1-\lambda(s))\frac{Q(s,q(s))}{[N(s),\Delta y(s),\dot{y}(q(s))]},\ B(s) := -\frac{[\dot{N}(s),\Delta y(s),\dot{y}(q(s))]}{[N(s),\Delta y(s),\dot{y}(q(s))]},$$

where we have used (2.2).

The goal is to obtain the uniqueness of PI lines. We start by choosing a vector $N(s)$ in such a way as to ensure that the denominator in (3.6) is never zero as long as $H(s,q(s))$ is a PI line. Denote the supremum (respectively, infimum) of all q such that $H(s,q)$ is a PI line by $q_{max}(s)$ (respectively, $q_{min}(s)$). Since $I=[a,b]$ is a compact interval, $q_{max}(s)$ and $q_{min}(s)$ are well-defined.

Our assumptions imply that the function $q_{max}(s)$ is continuous on (a,b). If $q_{max}(s)=b$ for some $s\in(a,b)$, then $q_{max}(t)\equiv b$ for all $t\in(s,b)$. If $q_{max}(s)<b$ for some $s\in(a,b)$, then

$$Q(q_{max}(s),s) = [y(q_{max}(s))-y(s),\dot{y}(s),\dot{y}(q_{max}(s))] = 0. \tag{3.7}$$

Differentiating (3.7) with respect to s gives

$$q'_{max}(s) = -\frac{[y(q_{max}(s))-y(s),\ddot{y}(s),\dot{y}(q_{max}(s))]}{[y(q_{max}(s))-y(s),\dot{y}(s),\ddot{y}(q_{max}(s))]}. \tag{3.8}$$

By assumption C2, $y(q_{max}(s))-y(s)$ and $\dot{y}(s)$ are never parallel. Hence, if the denominator in (3.8) is zero, together with (3.7) this implies

$$[y(q_{max}(s))-y(s),\dot{y}(q_{max}(s)),\ddot{y}(q_{max}(s))]=0,$$

which contradicts Proposition 2.3. Our argument implies that $q'_{max}(s)$ can have at most one point of discontinuity. If the discontinuity exists, then $q'_{max}(s)=0$ to the right of it, and $q'_{max}(s)$ is given by (3.8) to the left of it.

In a similar fashion we obtain that $q_{min}(s)$ is continuous, and $q'_{min}(s)$ is piecewise continuous on (a,b). Define

$$N_{max}(s) := \frac{y(q_{max}(s)) - y(s)}{|y(q_{max}(s)) - y(s)|},\ N_{min}(s) := \frac{y(q_{min}(s)) - y(s)}{|y(q_{min}(s)) - y(s)|},\ s \in (a,b). \tag{3.9}$$

Thus, $N_{max}(s)$ (resp., $N_{min}(s)$) is the unit vector along $H(s, q_{max}(s))$ (resp., $H(q_{min}(s), s)$).

Proposition 3.1. *Pick any $t \in (s, q_{max}(s))$. One has $[y(t)-y(s), \dot{y}(t), N_{max}(s)] \neq 0$, and the curve segments $C(s,t)$ and $C(t, q_{max}(s))$ are located on the opposite sides of the plane containing $H(s, q_{max}(s))$ and $y(t)$. Similarly, pick any $t \in (q_{min}(s), s)$. One has $[y(t) - y(s), \dot{y}(t), N_{min}(s)] \neq 0$, and the curve segments $C(t,s)$ and $C(q_{min}(s), t)$ are located on the opposite sides of the plane containing $H(q_{min}(s), s)$ and $y(t)$.*

Proof. We only prove the statements concerning $q_{max}(s)$. The other half of the proposition is completely analogous.

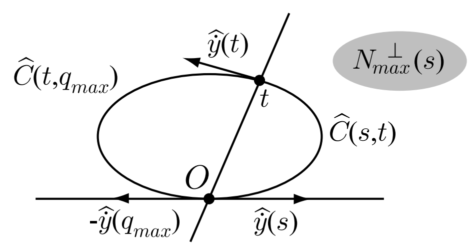

FIGURE 5. Projection onto the plane $N_{max}(s)^{\perp}$

The assertion $[y(t)-y(s), \dot{y}(t), N_{max}(s)] \neq 0$ follows immediately from statement (2) of Proposition 2.4 (see also its proof). This proposition also implies that any line, which contains O and passes between the rays $R_+(s_0)$ and $R_-(s_1)$, divides $\hat{C}(s, q_{max})$ into two segments located in the opposite half-planes (see Figure 5). This means that the curve segments $C(s,t)$ and $C(t, q_{max}(s))$ are located on the opposite sides of the plane containing $H(s, q_{max}(s))$ and $y(t)$. □

Next we determine the region where PI-lines, if exist, are unique. Even though the curve C is well-behaved locally, very little can be said about the global behavior of C. So we choose a "local" piece of C: $I_0 := [a_0, b_0] \subset (a,b)$. The word local is made precise later. For each $s \in I_0$ consider the curve $\hat{C}(s, q_{max})$ in the plane $N^{\perp}_{max}(s)$. By construction, $\hat{C}(s, q_{max})$ is closed. Let $Cyl_{max}(s)$ be the infinite open cylinder with axis $N_{max}(s)$, whose base is the interior of $\hat{C}(s, q_{max})$. In the same fashion we define the cylinders $Cyl_{min}(s)$ using $\hat{C}(q_{min}, s)$ and $N_{min}(s)$. Define U as the intersection of all such open cylinders:

$$U := \cap_{s \in I_0} \left(Cyl_{min}(s) \cap Cyl_{max}(s) \right). \tag{3.10}$$

If the curve turns too much, U can be empty. As an example, imagine a "slinky" toy. Locally it looks like a section of a helix. However if the slinky twists too much and the interval I_0 is sufficiently large, there can be no x that belongs to all the cylinders. We assume that a sufficiently "local" piece of C is taken, so $U \neq \varnothing$. Note that in the case of helix all cylinders $Cyl_{min}(s)$ and $Cyl_{max}(s)$ are identical, so (3.10) gives the usual domain inside the helix.

Proposition 3.2. *Pick $x \in U$. If x admits a PI-line, it is unique in the sense that there is no other PI-line with an endpoint inside I_0.*

Proof. Choose $N(s) := N_{max}(s)$ in (3.2). Since $x \in U$, x projects along $N(s)$ into the interior of $\hat{C}(s, q_{max})$ for any $s \in I_0$. Hence the functions $q(s)$, $\lambda(s)$, and the map $s \to x(s)$ (cf. (3.1), (3.2)) are well-defined on I_0. By Proposition 3.1, $[\Delta y(s), \dot{y}(q(s)), N(s)] \neq 0$ for any $s \in I_0$, i.e. $\varepsilon'(s)$ is smooth on I_0. By construction, $H(s, q(s))$ are PI-segments, so $Q(s, q(s)) \neq 0$ on I_0. Similarly, $\lambda(s) < 1$ on I_0.

Our argument implies that $A(s)$ (cf. (3.6)) is bounded away from zero and of constant sign on I_0. Consider now $B(s)$ (cf. (3.6)). As we already know, the denominator is bounded away from zero. Differentiating (3.9) gives

(3.11)
$$\begin{aligned}\dot{N}_{max}(s) =& \frac{1}{|y(q_{max}(s)) - y(s)|} \\ & \times \left\{ [\dot{y}(q_{max}(s)) q'_{max}(s) - \dot{y}(s)] - N\left(N \cdot [\dot{y}(q_{max}(s)) q'_{max}(s) - \dot{y}(s)]\right) \right\}.\end{aligned}$$

By assumption C1, C has no self-intersections, so $|y(q_{max}) - y(s)|$ is bounded away from zero. From (3.8) and the subsequent discussion, it follows that $q'_{max}(s)$ is bounded away from zero. Hence, $\dot{N}_{max}(s)$ is bounded, and $B(s)$ is bounded as well.

From the properties of $A(s)$ and $B(s)$ we get that $\varepsilon(s)$ cannot have more than one root on I_0. This follows immediately from the fact that the signs of $\varepsilon'(s)$ and $A(s)$ in a neighborhood of any s where $\varepsilon(s) = 0$ are the same. Hence x cannot have more than one PI-segment with $s_b(x) \in I_0$.

Choosing $N(s) := N_{min}(s)$ in (3.2) and repeating the same argument gives that x cannot have more than one PI-segment with $s_t(x) \in I_0$. $\square$

4. Reconstruction algorithm

In order to derive an inversion formula we need to study the curve C some more.

Proposition 4.1. *Let $H(s_0, s_1)$ be a (possibly maximal) PI-segment of C. Then $\hat{C}(s_0, s_1)$ has everywhere non-vanishing curvature.*

Proof. Recall that $\hat{C}(s_0, s_1)$ is smooth by Proposition 2.4. Pick any $t \in (s_0, s_1)$ and suppose the curvature vanishes there. This implies

$$[y(s_1) - y(s_0), \dot{y}(t), \ddot{y}(t)] = 0, \tag{4.1}$$

which means that $y(s_1) - y(s_0)$ is parallel to $\Pi_{osc}(t)$. Since $\tau(t) \neq 0$, $C(t - \epsilon, t)$ and $C(t, t + \epsilon)$ are on the opposite sides of $\Pi_{osc}(t)$ for some $\epsilon > 0$. By Proposition 2.3, $\Pi_{osc}(t)$ does not intersect $C(s_0, s_1)$ at any point other than $y(t)$. Hence $C(s_0, t)$ and $C(t, s_1)$ are on the opposite sides of $\Pi_{osc}(t)$. In particular, the line segment $H(s_0, s_1)$ intersects $\Pi_{osc}(t)$, which contradicts (4.1). If $t = s_0$ or $t = s_1$, the desired assertion follows immediately from Proposition 2.3. $\square$

Corollary 4.2. *Let $H(s_0, s_1)$ be a (possibly maximal) PI-segment of C. For any $x \in H(s_0, s_1)$ and $t \in (s_0, s_1)$, the vectors $\dot{y}(t)$ and $x - y(t)$ are not collinear.*

Proof. By Proposition 2.3, $\hat{C}(s_0, q_{max}(s_0))$ is strictly convex. $x \in H(s_0, s_1)$ implies that x projects into the domain bounded by $\hat{C}(s_0, q_{max}(s_0))$. Thus $\dot{y}(t)$ and $x - y(t)$ are not collinear. $\square$

Proposition 4.3. *Let $H(s_0, s_1)$ be a (possibly maximal) PI-segment of C. For any $x \in H(s_0, s_1)$ there exists the unique $s^*(x)$ such that $x \in \Pi_{osc}(s^*(x))$.*

Proof. As follows from the proof of Proposition 4.1, $\Pi_{osc}(t)$ intersects $H(s_0, s_1)$ for any $t \in [s_0, s_1]$. Hence we can write

$$y(s_0) + \lambda(t)(y(s_1) - y(s_0)) = y(t) + a(t)\dot{y}(t) + b(t)\ddot{y}(t) \tag{4.2}$$

for some scalar functions λ, a, and b. Differentiate (4.2) with respect to t, multiply the resulting equation by $\dot{y}(t) \times \ddot{y}(t)$ and solve for λ':

$$\lambda'(t) = b(t)\frac{[\dot{y}(t), \ddot{y}(t), \dddot{y}(t)]}{[y(s_1) - y(s_0), \dot{y}(t), \ddot{y}(t)]}. \tag{4.3}$$

Since the torsion of C is non-zero, the numerator in (4.3) does not vanish. From the proof of Proposition 4.1, the denominator in (4.3) is non-zero. By Corollary 4.2, $b(t) \neq 0, t \in (s_0, s_1)$. Hence $\lambda(t)$ is a smooth monotone function on $[s_0, s_1]$. Obviously, $\Pi_{osc}(s_0)$ (resp., $\Pi_{osc}(s_1)$) intersects $H(s_0, s_1)$ at $y(s_0)$ (resp., $y(s_1)$). Thus $\lambda(s_0) = 0$, $\lambda(s_1) = 1$, and the proposition is proven. □

Due to the containment property (statement (1) of Proposition 2.4), the curve $C(s, q_{max}(s))$ (resp., $C(s, q_{min}(s))$) is on one side of the plane passing through $y(s)$ and parallel to $\dot{y}(s)$ and $N_{max}(s)$ (resp., $N_{min}(s)$). This makes it very convenient to project $C(s, q_{max}(s))$ (resp., $C(s, q_{min}(s))$) onto a plane parallel to $\dot{y}(s)$ and $N_{max}(s)$ (resp., $N_{min}(s)$). The corresponding projections turn out to be smooth. Let $DP_+(s)$ (resp., $DP_-(s)$) denote a plane not passing through $y(s)$ and parallel to $\dot{y}(s)$ and $N_{max}(s)$ (resp., $N_{min}(s)$). The stereographic projection of $C(s, q_{max}(s))$ onto $DP_+(s)$ is denoted Γ_+, while the stereographic projection of $C(q_{min}(s), s)$ onto $DP_-(s)$ is denoted Γ_-.

Proposition 4.4. *Γ_+ and Γ_- are smooth and have nonvanishing curvature at every point.*

Proof. We only consider Γ_+. The statement about Γ_- is proven analogously. Suppose, for simplicity, that the origin is at $y(s)$, and the equation of $DP_+(s)$ is $x_3 = 1$. Thus, x_1 and x_2 are the coordinates on $DP_+(s)$. Let $x_1(t)$ and $x_2(t)$ be the coordinates of the projection of $y(t), t \in (s, q_{max}(s))$, onto $DP_+(s)$. Then

$$x_1(t) = \frac{y_1(t)}{y_3(t)},\ x_2(t) = \frac{y_2(t)}{y_3(t)}. \tag{4.4}$$

As is well-known,

$$\kappa(t) = \frac{\dot{x}_1^2}{(\dot{x}_1^2 + \dot{x}_2^2)^{3/2}}\left(\frac{\dot{x}_2}{\dot{x}_1}\right)'. \tag{4.5}$$

Differentiating (4.4) gives

$$\begin{aligned} \left(\frac{\dot{x}_2}{\dot{x}_1}\right)' &= \left(\frac{\dot{y}_2 y_3 - \dot{y}_3 y_2}{\dot{y}_1 y_3 - \dot{y}_3 y_1}\right)' \\ &= \frac{(\ddot{y}_2 y_3 - \ddot{y}_3 y_2)(\dot{y}_1 y_3 - \dot{y}_3 y_1) - (\dot{y}_2 y_3 - \dot{y}_3 y_2)(\ddot{y}_1 y_3 - \ddot{y}_3 y_1)}{(\dot{x}_1 y_3^2)^2} \\ &= \frac{1}{(\dot{x}_1 y_3^2)^2}\begin{vmatrix} y_1 & y_2 & y_3 \\ \dot{y}_1 & \dot{y}_2 & \dot{y}_3 \\ \ddot{y}_1 & \ddot{y}_2 & \ddot{y}_3 \end{vmatrix}. \end{aligned} \tag{4.6}$$

Substituting (4.6) into (4.5) and using (4.4) (recall that $y(s) = 0$ is the origin) gives the curvature of Γ_+:

$$\kappa(t) = \frac{\Phi(t,s)}{y_3^4(t)\left(\dot{x}_1^2(t) + \dot{x}_2^2(t)\right)^{3/2}}. \tag{4.7}$$

By the properties of $C(s, q_{max}(s))$ mentioned prior to this proposition, $y_3(t) \neq 0, t \in (s, q_{max}(s))$. Also, $y_3(s) = 0$ and, if $H(s, q_{max}(s))$ is maximal, $y_3(q_{max}(s)) = 0$. It remains to show that $\dot{x}_1^2(t) + \dot{x}_2^2(t) \neq 0$. This would also imply that Γ_+ is smooth. We argue by contradiction. Suppose $\dot{x}_1(t) = \dot{x}_2(t) = 0$. Then $\dot{y}_2 y_3 = \dot{y}_3 y_2$, $\dot{y}_1 y_3 = \dot{y}_3 y_1$. Consequently, $y(t) \times \dot{y}(t)$ is parallel to the x_3-axis. Thus, either both $y(t)$ and $\dot{y}(t)$ are parallel to $DP_+(s)$ or $y(t)$ and $\dot{y}(t)$ are parallel to each other. Both cases are impossible because of the convexity of $\hat{C}(s, q_{max}(s))$ (cf. Proposition 4.1). Since $\Phi(t,s) \neq 0$ for $t \in [s, q_{max}(s)]$ (cf. Proposition 2.3), the desired assertion is proven. □

Denote $L_0^+ := DP_+(s) \cap \Pi_{osc}(s)$. It is clear that L_0^+ is an asymptote of Γ_+: $\mathrm{dist}(\hat{y}(t), L_0^+) \to 0$ as $t \to s^+$. Similarly, $L_0^- := DP_-(s) \cap \Pi_{osc}(s)$ is an asymptote of Γ_-: $\mathrm{dist}(\hat{y}(t), L_0^-) \to 0$ as $t \to s^-$.

Fix $x \in U$, which admits a PI-line. Let $I_{PI}(x) = [s_b(x), s_t(x)]$ be the PI-interval of x. Let $\hat{x}$ denote the projection of x onto a detector plane. Frequently it is convenient to identify detector planes by introducing systems of coordinates that depend smoothly on s. This allows to identify all $DP_+(s)$ and, separately, all $DP_-(s)$. Since $x \in U$, x does not belong to any plane passing through $y(s)$ and parallel to $DP_+(s)$ or $DP_-(s)$, where $s \in I_{PI}(x)$. Hence propositions 4.3 and 3.2 immediately imply the following statement.

Corollary 4.5. *As s moves along $I_{PI}(x)$, the point $\hat{x}$ traces smooth curves on $DP_+(s)$ and $DP_-(s)$. $\hat{x}$ is between $\Gamma_+(s)$ and L_0^+ on $DP_+(s)$ if and only if $s \in (s_b(x), s^*(x))$, and $\hat{x}$ is between L_0^- and $\Gamma_-(s)$ on $DP_-(s)$ if and only if $s \in (s^*(x), s_t(x))$.*

Loosely speaking, Corollary 4.5 can be stated as follows: $\hat{x}$ is between $\Gamma_+(s)$ and $\Gamma_-(s)$ if and only if $s \in I_{PI}(x)$.

Following [Kat02, Kat04b], choose any $\psi \in C^\infty(\mathbb{R}^+)$ with the properties

$$\begin{aligned} &\psi(0) = 0;\ 0 < \psi'(t) < 1,\ t \geq 0, \\ &\psi'(0) = 0.5;\ \psi^{(2k+1)}(0) = 0,\ k \geq 1. \end{aligned} \tag{4.8}$$

Suppose s, s_1, and s_2 are related by

$$s_1 = \begin{cases} \psi(s_2 - s) + s, & s_2 \geq s, \\ \psi(s - s_2) + s_2, & s_2 < s. \end{cases} \tag{4.9}$$

¿From (4.8), $s_1 = s_1(s, s_2)$ is a C^∞ function of s and s_2. Conditions (4.8) are easy to satisfy. One can take, for example, $\psi(t) = t/2$, and this leads to

$$s_1 = (s + s_2)/2. \tag{4.10}$$

Denote also

$$u(s,s_2) = \frac{(y(s_1)-y(s))\times(y(s_2)-y(s))}{|(y(s_1)-y(s))\times(y(s_2)-y(s))|}\text{sgn}(s_2-s),$$
$$q_{min}(s) < s_2 < q_{max}(s), s_2 \neq s, \tag{4.11}$$
$$u(s,s_2) = \frac{\dot y(s)\times\ddot y(s)}{|\dot y(s)\times\ddot y(s)|},\ s_2 = s.$$

In the same way as in [Kat04b], we prove that $u(s,s_2)$ is a C^∞ vector function of its arguments. Let $\Pi(s,s_2)$ be the plane through $y(s), y(s_2)$, and $y(s_1(s,s_2))$. Intersection of $\Pi(s,s_2)$ with $DP_+(s)$ if $s < s_2 < q_{max}(s)$ or with $DP_-(s)$ if $q_{min}(s) < s_2 < s$ is called a filtering line and denoted $L(s,s_2)$.

Fix $x \in U$, which admits a PI-line, and $s \in I_{PI}(x)$. Find $s_2 \in I_{PI}(x)$ such that $\Pi(s,s_2)$ contains x. More precisely, we have to solve for s_2 the following equation

$$(x-y(s))\cdot u(s,s_2) = 0,\ s_2 \in I_{PI}(x). \tag{4.12}$$

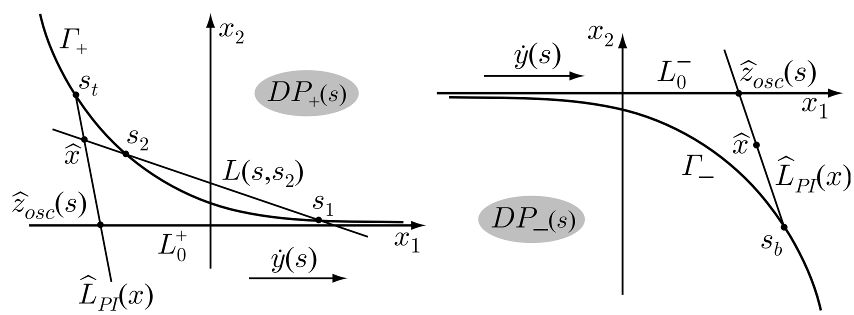

FIGURE 6. Detector planes $DP_+(s)$ (left panel) and $DP_-(s)$ (right panel).

Recall that $\dot y(s)$ is parallel to $DP_+(s)$ and $DP_-(s)$. For convenience, we choose the x_1- and x_2-axes so that

(1) $\dot y(s)$ and the x_1-axis are parallel and point in the same direction;
(2) The equation of $\Pi_{osc}(s)$ is $x_2 = 0$;
(3) On $DP_+(s)$, Γ_+ is located in the half-plane $x_2 > 0$;
(4) On $DP_-(s)$, Γ_- is located in the half-plane $x_2 < 0$.

Figure 6 illustrates the two detector planes.

The advantage of planes $DP_+(s)$ and $DP_-(s)$ is that the segments $C(s,q_{max}(s))$ and $C(q_{min}(s),s)$ are projected onto them as continuous curves with positive curvature. If C is a helix, the two segments become the usual 2π-segments $C(s,s+2\pi)$ and $C(s-2\pi,s)$. This makes it very convenient when describing how to choose filtering lines in a shift-invariant FBP algorithm. On the other hand, the disadvantage is that the two segments are projected onto two different planes. This makes it difficult to adapt the proofs from [Kat04b, Kat02] to the present more general situation. Fortunately, the difficulty can be resolved. Given $x \in U$ with the PI-interval $I_{PI}(x) = [s_b(x), s_t(x)]$, we can find a family of "detector planes" such that for any $s \in I_{PI}(x)$ the entire PI-segment of x, $C(s_b(x), s_t(x))$, projects onto them in exactly the same way as in the case of a regular constant pitch helix. There is no guarantee that the larger segment $C(q_{min}(s), q_{max}(s))$ (which is equivalent to two adjacent turns of a helix) projects well onto the planes, but this is not needed.

Let $DP(s), s \in I_{PI}(x)$, be a plane not passing through $y(s)$ and parallel to $\dot{y}(s)$ and $N_{max}(s_b(x))$. Using the convexity of $C(s_b(x), s_t(x)) \subset C(s_b(x), q_{max}(s_b(x)))$ (cf. proposition 4.1 and Figure 5) and repeating the proof of proposition 4.4, we establish that the stereographic projection of $C(s_b(x), s_t(x))$ onto $DP(s)$ has all the usual properties as in the constant-pitch helix case. More precisely, the projections of $C(s_b(x), s)$ and $C(s, s_t(x))$ are concave down and up, respectively, they share the usual asymptote $DP(s) \cap \Pi_{osc}(s)$, are located on the opposite sides of the latter, etc. Thus, using the same argument as in [Kat04b, KBH04], we immediately obtain the following result.

Proposition 4.6. *The solution s_2 to (4.12) exists, is unique, and depends smoothly on s.*

The following result shows that filtering lines are shared by sufficiently many points $x \in U$. The planes $DP(s)$ used for the proof of proposition 4.6 are selected separately for each x, so they do necessarily work for all x in a large subset of U. Thus we have to go back to the planes $DP_+(s)$ and $DP_-(s)$.

Proposition 4.7. *All $x \in U$ that project onto any line $L(s, s_2), s < s_2 < q_{max}(s)$, on $DP_+(s)$ to the left of s_2 or onto $L(s, s_2), q_{min}(s) < s_2 < s$, on $DP_-(s)$ to the right of s_2, share $L(s, s_2)$ as their filtering line.*

Proof. We only consider the case when $s_2 > s$, i.e. $\hat{x} \in DP_+(s)$. The other case can be considered analogously. We have $s_t(x) \in \Gamma_+$. By corollary 4.5, $\hat{x}$ appears between L_0^+ and Γ_+. From the proof of proposition 4.1, $\Pi_{osc}(s)$ intersects the PI-segment of x, $H(s_b(x), s_t(x))$. Let $z_{osc}(x)$ denote the point of intersection. Let $\Pi_{max}(s)$ be the plane through $y(s)$ and parallel to $\dot{y}(s)$ and $N_{max}(s)$. The intersection of the line through $L_{PI}(x)$ and $\Pi_{max}(s)$ is denoted $z_{max}(s)$. Clearly, $z_{osc}(s) = z_{max}(s)$ when $s = s_b(x)$. From the proof of proposition 4.3, $z_{osc}(s)$ moves toward $y(s_t(x))$ along $L_{PI}(x)$ as s increases from $s_b(x)$ to $s_t(x)$. From the convexity of $\hat{C}(s, q_{max}(s))$ (cf. Figure 5), it is easy to obtain that in a neighborhood of $s = s_b(x)$ the point $z_{max}(s)$ moves away from $H(s_b(x), s_t(x))$ as s increases. If for some $s \in (s_b(x), s_t(x))$ the points $z_{osc}(x)$ and $y(s_t(x))$ are on the opposite sides of $\Pi_{max}(s)$, then the point $z_{max}(s)$ enters the line segment $[z_{osc}(x), y(s_t(x))]$ for some $s = s_0 \in (s_b(x), s_t(x))$. Hence, either (i) $z_{osc}(s_0) = z_{max}(s_0)$ or (ii) $y(s_t(x)) = z_{max}(s_0)$. From proposition 2.3, $[y(q_{max}(s_0)) - y(s_0), \dot{y}(s_0), \ddot{y}(s_0)] \neq 0$, so (i) implies that $z_{osc}(s_0) - y(s_0)$ and $\dot{y}(s_0)$ are collinear, which contradicts corollary 4.2. In case (ii), $y(s_t(x)) \in \Pi_{max}(s_0)$, which contradicts the containment property.

Hence $\hat{L}_{PI}(x)$, the projection of $H(s_b(x), s_t(x))$ onto $DP_+(s)$, intersects L_0^+. More precisely, the projection of the line segment $[z_{osc}(x), y(s_t(x))] \subset L_{PI}(x)$ is a continuous line segment that connects Γ_+ and L_0^+ (see Figure 6). Note that proposition 4.3 implies $z \in [z_{osc}(x), y(s_t(x))]$ if $s < s^*(x)$. It turns out that $\hat{L}_{PI}(x)$ does not intersect Γ_+ at any point other than $s_t(x)$. Suppose there is an additional intersection point t. Thus the plane through $y(s)$ and $H(s_b(x), s_t(x))$ intersects $C_{PI}(x)$ at four points: $s_b(x), t, s$, and $s_t(x)$, and this contradicts corollary 2.5.

If x projects onto $L(s, s_2)$ to the left of s_2, we make two observations: (i) $\hat{x}$ is between L_0^+ and Γ_+ on $DP_+(s)$; and (ii) $s_2 < s_t$ (due to the properties of $\hat{L}_{PI}(x)$ that we just established). From (i) and corollary 4.5, $s \in I_{PI}(x)$. From (ii), $s_2 \in (s, s_t(x))$, so by (i) $s_2 \in I_{PI}(x)$. By construction, s_2 was chosen to satisfy (4.8), (4.9) and $(x - y(s)) \cdot u(s, s_2) = 0$. We have just shown that $s, s_2 \in I_{PI}(x)$. This proves that $L(s, s_2)$ is the filtering line for x. $\square$

By proposition 4.7, our construction defines $s_2 := s_2(s,x)$ and, consequently, $u(s,x) := u(s, s_2(s,x))$. Let $D_f(s,\Theta) = \int_0^\infty f(y(s)+t\Theta)dt$, $|\Theta|=1$, denote the cone beam transform of f. The main result of the paper is the following theorem.

Theorem 4.8. *Let C be a curve (2.1), which satisfies conditions C1–C4. Let $I_0 \subset I$ be an interval, such that the set U defined by (3.10) is non-empty. For any $f \in C_0^\infty(U)$ and $x \in U$ which admits a PI line one has*

$$f(x) = -\frac{1}{2\pi^2}\int_{I_{PI}(x)} \frac{1}{|x-y(s)|}\int_0^{2\pi} \frac{\partial}{\partial q} D_f(q, \Theta(s,x,\gamma))\bigg|_{q=s} \frac{d\gamma}{\sin\gamma} ds, \tag{4.13}$$

where $e(s,x) := \beta(s,x) \times u(s,x)$ and $\Theta(s,x,\gamma) := \cos\gamma\beta(s,x) + \sin\gamma e(s,x)$.

Proof. Corollaries 2.5, 2.6, 4.5, and Propositions 4.1, 4.3, 4.4, and 4.6 imply that locally, i.e. in a neighborhood of $I_{PI}(x)$, the curve C behaves in essentially the same way as the usual helix. Hence the same argument as in [Kat04b, KBH04] can be used to prove that (4.13) holds. □

Proposition 4.7 implies that (4.13) is of the efficient shift-invariant FBP form.

5. Numerical experiments

Numerical experiments are conducted using flat detector geometry. The simulation parameters are summarized in Table 1. The algorithm is implemented in the native coordinates following [NPH03]. We use the virtual detector, which always contains the x_3-axis. The clock phantom (see, e.g., [KBH04]) is chosen for reconstruction. The background cylinder is at 0 HU, the spheres are at 1000 HU, and the air is at -1000 HU.

Parameter	Value	Units
Views per rotation	1000	
Number of detector columns	1201	
Number of detector rows	161	
Detector pixel size	0.5 × 0.5	mm^2

Table 1. Simulation parameters

Two source trajectories have been used. The first one is a variable radius helix given by the formula:

$$y(s) = \left(R(s)\cos s, R(s)\sin s, \frac{h_0}{2\pi}s\right),\ R(s) = R(1+0.3\sin(s/3)), \tag{5.1}$$

where $R = 600$mm, and table feed per turn is $h_0 = 35$mm. The projection of this trajectory onto the plane $x_3 = 0$ for $s \in [-2\pi, 2\pi]$ is shown in Fig. 7. The boundary of the set U is calculated according to (3.10). The cross-section of the boundaries of cylinders $Cyl_{min}(s)$ and $Cyl_{max}(s)$ with the plane $x_3 = 0$ is shown in Fig. 9 (left panel). The solid circle of radius $r = 240$mm shows the boundary of the clock phantom, and the dashed circle is of the maximum radius $r \approx 374$mm that fits inside the cross-section of U. The result of reconstruction is shown in Fig. 8.

The second experiment is carried out using the variable radius and variable pitch helix given by:

$$y(s) = \left(R(s)\cos s, R(s)\sin s, \frac{h(s)}{2\pi}s\right),\ h(s) = h_0\left(1+\frac{\sin(s/2)}{s}\right). \tag{5.2}$$

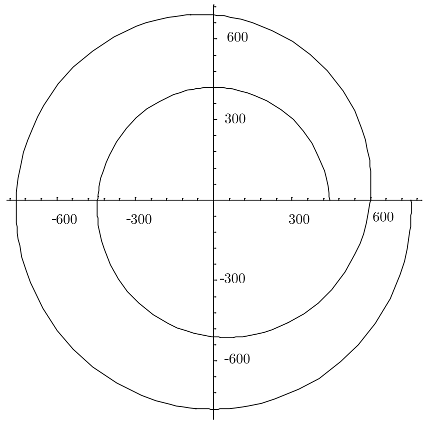

FIGURE 7. Projection of the source trajectory in (5.1) onto the xy-plane.

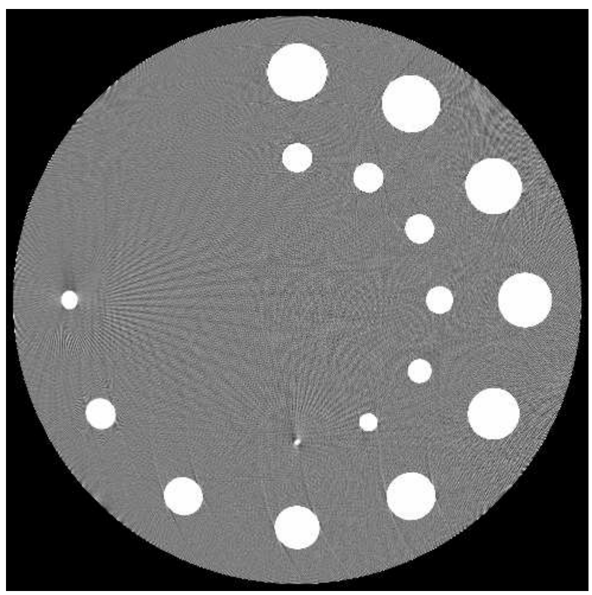

FIGURE 8. Reconstruction of the clock phantom from trajectory (5.1): slice $x_3 = 0$, WL=0 HU, WW=100 HU.

Here $R(s)$ and h_0 are the same as in (5.1). The cross-section of the boundaries of cylinders $Cyl_{min}(s)$ and $Cyl_{max}(s)$ with the plane $x_3 = 0$ is shown in Fig. 9 (right panel). Again, the solid circle of radius $r = 240$mm shows the boundary of the clock phantom, and the dashed circle is of the maximum radius $r \approx 348$mm that fits inside the cross-section of U. The results of the reconstruction are shown in Fig. 10.

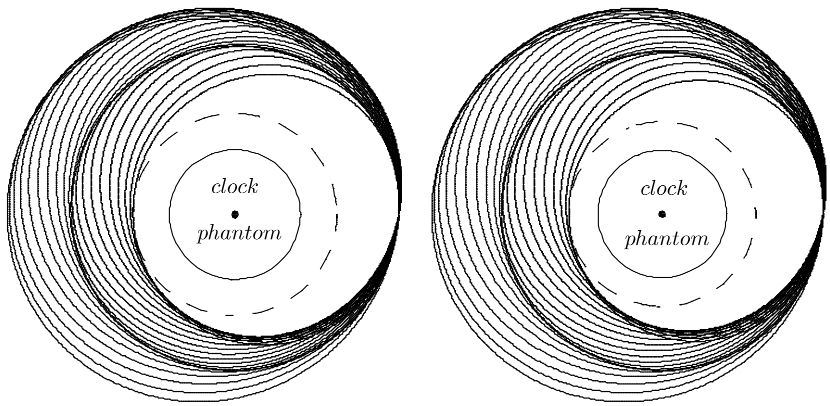

FIGURE 9. Cross-section of boundaries of cylinders $Cyl(s)$ from (3.10) for trajectory (5.1) (left panel) and trajectory (5.2) (right panel).

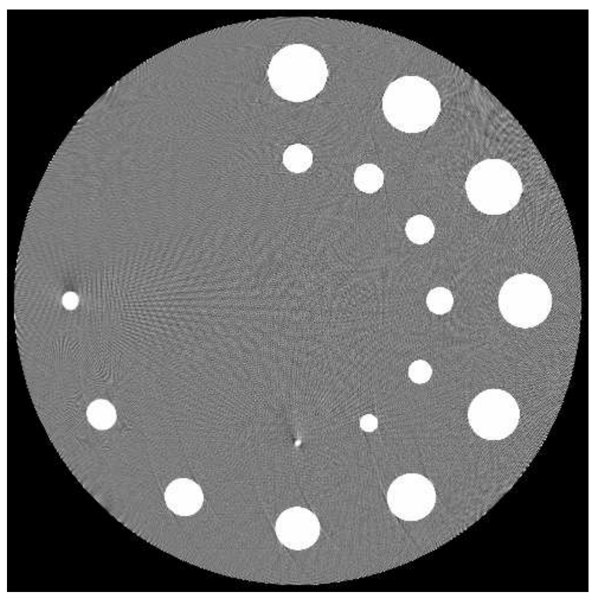

FIGURE 10. Reconstruction of the clock phantom from trajectory (5.2): slice $z = 0$, WL=0 HU, WW=100 HU.

REFERENCES

[BKP05] C. Bontus, T. Köhler, and R. Proksa, *EnPiT: filtered back-projection algorithm for helical CT using an n-Pi acquisition*, IEEE Transactions on Medical Imaging **24** (2005), 977–986.

[CZLN06] G.-H. Chen, T.-L. Zhuang, S. Leng, and B. E. Nett, *Shift-invariant and mathematically exact cone-beam FBP reconstruction using a factorized weighting function*, IEEE Transactions on Medical Imaging (2006), submitted.

[Kat02] A. Katsevich, *Analysis of an exact inversion algorithm for spiral cone-beam CT*, Physics in Medicine and Biology **47** (2002), 2583–2598.

[Kat04a] ———, *Image reconstruction for the circle and line trajectory*, Physics in Medicine and Biology **49** (2004), 5059–5072.

[Kat04b] ———, *An improved exact filtered backprojection algorithm for spiral computed tomography*, Advances in Applied Mathematics **32** (2004), 681–697.

[Kat04c] ———, *On two versions of a 3π algorithm for spiral CT*, Physics in Medicine and Biology **49** (2004), 2129–2143.

[Kat05] ———, *Image reconstruction for the circle and arc trajectory*, Physics in Medicine and Biology **50** (2005), 2249–2265.

[Kat06] ———, *3PI algorithms for helical computer tomography*, Advances in Applied Mathematics **21** (2006), 213–250.

[KBH04] A. Katsevich, Samit Basu, and Jiang Hsieh, *Exact filtered backprojection reconstruction for dynamic pitch helical cone beam computed tomography*, Physics in Medicine and Biology **49** (2004), 3089–3103.

[KBK06] Th. Köhler, C. Bontus, and P. Koken, *The Radon-split method for helical cone-beam CT and its application to nongated reconstruction*, IEEE Transactions on Medical Imaging **25** (2006), 882–897.

[KK06] M. Kapralov and A. Katsevich, *A 1PI algorithm for helical trajectories that violate the convexity condition*, Inverse Problems (2006), to appear.

[KL03] A. Katsevich and G. Lauritsch, *Filtered backprojection algorithms for spiral cone beam CT*, Sampling, Wavelets, and Tomography (John Benedetto and Ahmed Zayed, eds.), Birkhauser, 2003, pp. 255–287.

[KND00] H. Kudo, F. Noo, and M. Defrise, *Quasi-exact filtered backprojection algorithm for long-object problem in helical cone-beam tomography*, IEEE Transactions on Medical Imaging **19** (2000), 902–921.

[NPH03] F. Noo, J. Pack, and D. Heuscher, *Exact helical reconstruction using native cone-beam geometries*, Physics in Medicine and Biology **48** (2003), 3787–3818.

[PN05] J. D. Pack and F. Noo, *Cone-beam reconstruction using 1D filtering along the projection of M-lines*, Inverse Problems **21** (2005), 1105–1120.

[PNC05] J. D. Pack, F. Noo, and R. Clackdoyle, *Cone-beam reconstruction using the backprojection of locally filtered projections*, IEEE Transactions on Medical Imaging **24** (2005), 1–16.

[SZP05] E.Y. Sidky, Y. Zou, and X. Pan, *Minimum data image reconstruction algorithms with shift-invariant filtering for helical, cone-beam CT*, Physics in Medicine and Biology **50** (2005), 1643–1657.

[YLKK06] H. Yang, M. Li, K. Koizumi, and H. Kudo, *Exact cone beam reconstruction for a saddle trajectory*, Physics in Medicine and Biology **51** (2006), 1157–1172.

[YZW04] Y. Ye, J. Zhu, and G. Wang, *Geometric studies on variable radius spiral cone-beam scanning*, Medical Physics **31** (2004), 1473–1480.

[YZYW05a] Y. Ye, S. Zhao, H. Yu, and G. Wang, *A general exact reconstruction for cone-beam CT via backprojection-filtration*, IEEE Transactions on Medical Imaging **24** (2005), 1190–1198.

[YZYW05b] H. Yu, S. Zhao, Y. Ye, and G. Wang, *Exact BPF and FBP algorithms for nonstandard saddle curves*, Medical Physics **32** (2005), 3305–3312.

[ZLNC04] T. Zhuang, S. Leng, B. E. Nett, and G. Chen, *Fan-beam and cone-beam image reconstruction via filtering the backprojection image of differentiated projection data*, Physics in Medicine and Biology **49** (2004), 1643–1657.

[ZPXW05] Y. Zou, X. Pan, D. Xia, and G. Wang, *PI-line-based image reconstruction in helical cone-beam computed tomography with a variable pitch*, Medical Physics **32** (2005), 2639–2648.